Proceedings of IDETC/CIE 2005
ASME 2005 International Design Engineering Technical Conferences and Computers and Information in Engineering Conference
September 24-28, 2005, Long Beach, California, USA

DETC2005-85309

A STUDY OF THE RELATIONSHIP BETWEEN THE DYNAMIC FACTOR AND THE DYNAMIC TRANSMISSION ERROR OF SPUR GEAR PAIRS

Tamminana, V. K.
Graduate Assistant
Department of Mechanical Engineering
The Ohio State University
650 Ackerman Road, Columbus, OH, 43202

Kahraman, A.
Associate Professor
Department of Mechanical Engineering
The Ohio State University
650 Ackerman Road, Columbus, OH, 43202

Vijayakar, S.
Advanced Numerical Solutions,
3956 Brown Park Drive Suite B
Hilliard, OH 43026

Abstract

In this study, two different dynamic models, a finite elements-based deformable-body model and a simplified discrete model, are developed to predict dynamic behavior of spur gear pairs. Dynamic transmission error (*DTE*) and dynamic factors (*DF*) defined based on the gear mesh loads, tooth loads and bending stresses are computed for a number of unmodified and modified spur gears within a wide range of rotational speed for different involute contact ratios and torques. Both models are validated by comparing their *DTE* predictions with experimental data obtained from a set of tests using spur gear having unmodified and modified tooth profiles. The predicted *DF* and *DTE* values are related to each other through simplified formulas. Impact of nonlinear behavior such as tooth separations and jump discontinuities on *DF* is also quantified.

1. Introduction

Dynamic behavior of gear systems is important for two main reasons. One reason is the durability of the gear pair. Forces acting at the gear meshes and bearings under dynamic conditions might be many times larger than corresponding quasi-static forces. As a result of this, stresses, and hence, bending and contact fatigue lives of a gear set are influenced by its vibratory behavior. Gear design standards incorporate a dynamic rating factor [1] in an attempt to account for such dynamic effects. The second reason that makes the dynamic behavior relevant is the noise generated by the gear set. Time-varying dynamic gear mesh and bearing forces are transmitted to surrounding structures through the housing and the mounts to cause gear whine noise. Therefore, large vibration amplitudes typically result in higher noise levels as well.

Most of the theoretical and experimental studies to date were performed with only one of the reasons (noise or durability) in mind. Starting with the dynamic models, a large number of them have been developed over the years as reviewed by Ozguven and Houser [2], Blankenship and Singh [3] and Wang et al [4]. A great majority of these studies uses discrete models to predict the parameters that might be useful in quantifying how noisy the gear set would be. A few examples from a large number of studies of this type are referenced here to represent this approach [5-13]. A discrete gear mesh interface model consists of a mesh stiffness element (mostly a periodically time-varying function to represent the fluctuation of the number of tooth pairs in contact as gears rotate) and a viscous damper that are both applied along the line of action of the spur gear pair. A clearance type constraint to represent backlash induced tooth separations and an external displacement excitation to represent gear profile errors and intentional tooth modifications were included in some of these models. Both mesh stiffness function and displacement excitation would be determined by using a static-elastic gear analysis model. One commonly used form output from these models was the dynamic transmission error (*DTE*) that is defined as

$$DTE = r_1\theta_1(t) + r_2\theta_2(t) \tag{1}$$

which represents the motion transfer error along the line of action of gears where r_1 and r_2 are the base radii of gears 1 and 2, and θ_1 and θ_2 are the angular displacements. This

is the dynamic equivalent of the better-known Static Transmission Error (*STE*). A number of major experimental studies on spur gear dynamics including Munro [14], Umezawa et al [15] and Kahraman and Blankenship [16-20] used *DTE* as the metric to quantify the dynamic behavior. These experimental studies demonstrated clearly that mesh stiffness fluctuations and gear backlash must be included in an analysis of a spur gear pair as it acts as a parametrically excited nonlinear system in dynamic terms. These experimental studies guided many modeling efforts and were used for modal validation efforts [6-8,16,17].

Several other investigations predicted dynamic forces acting at the gear mesh to quantify the dynamic behavior [21-27]. Since the gear mesh damping force is very small compared to the gear mesh spring force, the dynamic gear mesh force (*DMF*) can be approximated as the product of the gear mesh stiffness and *DTE*. Dynamic factor was defined in these studies as $DF = (DMF)_{\max} / SMF$ where $(DMF)_{\max}$ is the maximum value of the dynamic mesh force and *SMF* is the static mesh force transmitted by the gear pair. The main shortcoming of these models is that they were capable of predicting only *DF* based on the gear mesh forces as defined earlier while the durability of the system would require prediction of the state of gear stresses under dynamic conditions. An accurate prediction of dynamic stresses requires the dynamic model that includes flexible teeth, gear blanks and contacts, all of which are possible via a deformable body model. There are recent deformable-body spur gear dynamics models (e.g. reference [28]), which were shown to compare well with *DTE* measurements of some of the studies cited earlier [16-20]. However, these deformable-body models did not focus on *DF* or gear stresses as a part of the dynamic behavior. Similarly, experimental studies that focused on the measurement of the dynamic bending gear stresses [29] are yet to be related to any dynamic model.

This study attempts to bridge this apparent gap between gear durability concerns and gear dynamics models. For this purpose, two different dynamic models, a deformable-body model and a discrete model, will be developed. The deformable-body model will have the capacity of predicting both *DTE* and *DF* based on mesh and tooth forces as well as dynamic gear tooth bending stresses. The discrete model will rely on the deformable-body model for computation of gear mesh parameters under quasi-static conditions and will predict both *DTE* and *DF* based on mesh and tooth forces. The experimental data collected using the test rig described in Kahraman and Blankenship [16-20] will be employed to validate both models by comparing predicted and measured *DTE* values. The validation matrix will include several gear sets having different involute contact ratios and tooth profile modifications operating within a wide range of rotational speed at different applied loads. The validated models will then be used for two specific purposes. First, *DTE* values will be related to *DF* values based on (i) gear mesh forces, (ii) tooth forces, and (iii) bending stresses. Simplified relationships between *DTE* and different forms of *DF* will be proposed, with the intent that extensive experimental and theoretical *DTE* database available in the literature can be related to the durability of the gear sets. Secondly, impact of tooth separations and jump discontinuities due to backlash on gear stresses will be quantified. Such effects were studied in the past using *DTE* for solely noise purposes, and their impact on gear durability is yet to be understood.

2. Dynamic Models

2.1 Deformable-body Model. The width of the contact zone in typical gear applications is two orders of magnitude smaller than the dimensions of the gear teeth themselves, requiring a very fine mesh inside the contact zone. The location of the contact zone changes as the gears enter and exit the mesh. When conventional FE methods are used, besides having an extremely refined mesh, re-meshing is necessary for every contact position.

A gear contact analysis model [30], which is the same model used in reference [28], will be used here to perform a deformable-body dynamic analysis of a spur gear pair. The model divides the gear into a near-field region near the contact, and a far-field region away from the contact. The finite element (FE) method is used to compute relative deformations and stresses for points in the far-field, and a semianalytical deformation model based on the Bousinesq and Cerruti solutions is used in the near field within the contact zones [31]. This approach does not require a highly refined mesh at the contacting tooth surfaces, reducing the computational effort compared to conventional FE models which require a refined mesh at gear tooth region, limiting the model to static analysis only. Therefore, the model used here allows a more refined and comprehensive study of spur gear dynamics than the conventional FE models. The tooth surfaces are modeled by a large number of nodes representing the involute shape and surface modifications. The model illustrated in Figure 1 makes it unnecessary to locally refine the FE mesh near the contact, and re-mesh the finite elements for each contact position.

A reference frame is attached to the pinion and gear and the finite element computations are done for each of them separately. The mesh stiffness and mesh contact forces, comprising the dynamic excitation for the system, are evaluated internally at each time step [31]. Contact conditions are handled as linear inequality constraints whose solution is obtained by a revised Simplex solver.

Contact analysis determines the contact conditions between the pinion and gear at each time step. In the absence of rigid body motion, the FE displacement vector $\mathbf{x}_{fi}$ for gear i satisfy the linear system of differential equations [28]:

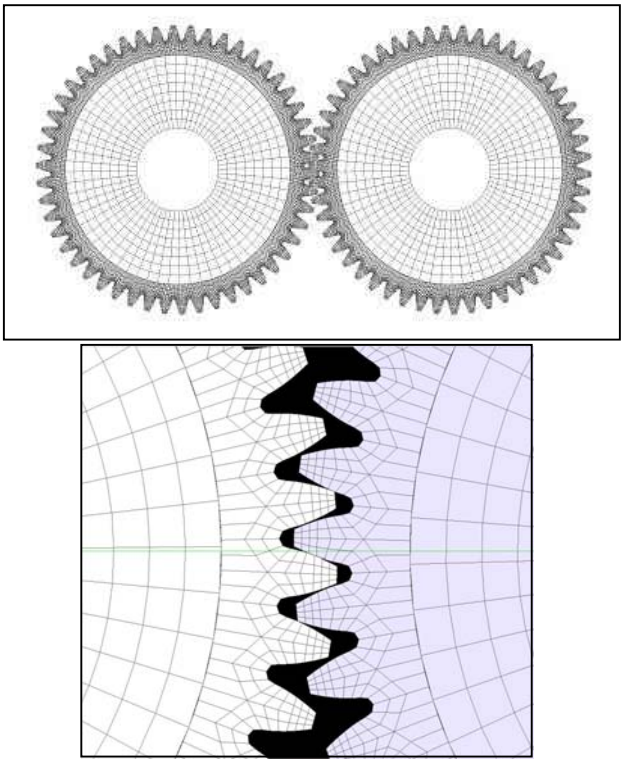

Figure 1: Deformable-body dynamic model of an example spur gear pair.

$$\mathbf{M}_{ffi}\ddot{\mathbf{x}}_{fi} + \mathbf{C}_{ffi}\dot{\mathbf{x}}_{fi} + \mathbf{K}_{ffi}\mathbf{x}_{fi} = \mathbf{f}_{fi} \tag{2}$$

where $\mathbf{f}_{fi}$ is the vector of external loads. Rayleigh's damping model is used here in the form $\mathbf{C}_{ffi} = \mu\mathbf{M}_{ffi} + \eta\mathbf{K}_{ffi}$ where μ and η are constant coefficients. If rigid body motion is considered, and if we represent the rigid body degrees of freedom by $\mathbf{x}_{ir}$ we replace (2) by

$$\begin{bmatrix} \mathbf{M}_{ffi} & \mathbf{M}_{fri} \\ \mathbf{M}_{rfi} & \mathbf{M}_{rri} \end{bmatrix} \begin{Bmatrix} \ddot{\mathbf{x}}_{fi} \\ \ddot{\mathbf{x}}_{ri} \end{Bmatrix} + \begin{bmatrix} \mathbf{C}_{ffi} & \mathbf{C}_{fri} \\ \mathbf{C}_{rfi} & \mathbf{C}_{rri} \end{bmatrix} \begin{Bmatrix} \dot{\mathbf{x}}_{fi} \\ \dot{\mathbf{x}}_{ri} \end{Bmatrix} + \begin{bmatrix} \mathbf{K}_{ffi} & \mathbf{K}_{fri} \\ \mathbf{K}_{rfi} & \mathbf{K}_{rri} \end{bmatrix} \begin{Bmatrix} \mathbf{x}_{fi} \\ \mathbf{x}_{ri} \end{Bmatrix} = \begin{Bmatrix} \mathbf{f}_{fi} \\ \mathbf{f}_{ri} \end{Bmatrix} \tag{3}$$

The equations for the pinion ($i = 1$) and the gear ($i = 2$) are assembled into the matrix equation of motion

$$\mathbf{M}\ddot{\mathbf{x}} + \mathbf{C}\dot{\mathbf{x}} + \mathbf{K}\mathbf{x} = \mathbf{F} \tag{4}$$

The deformable body model employs a time-discretization scheme based on Newmark method [30], as used successfully in previous studies [28, 32].

2.2 Discrete Parameter Model. The proposed discrete model is based on an existing gear dynamics model developed by one of the authors [16]. This non-linear, time varying model is shown in Figure 2. It consist of two rigid wheels of polar mass moments of inertia of I_1 and I_2, and base radii of r_1 and r_2. The gear mesh interface is represented by a periodically time-varying mesh stiffness function $k(t)$ and a viscous damper c. Here $k(t)$ takes into account the parametric excitation due to the mesh stiffness variation caused by the fluctuation of number of tooth pairs in contact. A clearance type non-linear restoring function g is included to represent the gear backlash of magnitude $2b$. An external displacement excitation $e(t)$ is also applied at the gear mesh interface to represent manufacturing errors and intentional modifications of the tooth profile. Friction forces at the gear tooth contact are neglected, and the shafts and bearings supporting the gears are assumed to be rigid. With these assumptions, the governing equation of motion represented by the single-degree-of-freedom dynamic model shown in Figure 2 is given for a coordinate $x(t) = r_1\theta_1(t) + r_2\theta_2(t) - e(t)$ as

$$m_e\,\ddot{x} + c\,\dot{x} + k(t)g[x(t)] = F - m_e\ddot{e}(t)\,, \tag{5a}$$

$$g[x(t)] = \begin{cases} x(t) - b, & x(t) > b, \\ 0, & |x(t)| \le b, \\ x(t) + b, & x(t) < b, \end{cases} \tag{5b}$$

$$F = m_e\left(\frac{T_1 r_1}{I_1} + \frac{T_2 r_2}{I_2}\right), \quad m_e = \frac{I_1 I_2}{I_1 r_2^2 + I_2 r_1^2} \tag{5c,d}$$

where an overdot denotes differentiation with respect to time t, and T_1 and T_2 are constant torque values applied to the pinion and gear, respectively. Torque fluctuations are not considered in this model as the experimental setup described later is suitably designed to maintain a constant torque value. In eq. (5), $x(t)$ represents the difference between *DTE* defined in eq. (1) and the unloaded *STE*.

The governing eq. (5) can be non-dimensionalized by defining a characteristic frequency $\omega_n = \sqrt{k_m/m_e}$ and a characteristic displacement b (half backlash). Here ω_n is the undamped natural frequency of the corresponding linear time-variant system where k_m is the mesh stiffness, i.e. $k(t) = k_m + k_a(t)$. Defining a dimensionless time $\tau = \omega_n t$, a viscous damping ratio $\zeta = c/(2\sqrt{m_e k_m})$ and dimensionless displacements $\bar{x}(\tau) = x(\tau)/b$ and $\bar{e}(\tau) = e(\tau)/b$, one obtains

$$\bar{x}'' + 2\zeta\bar{x}' + \left[1 + \bar{k}_a(\tau)\right]\; g[\bar{x}(\tau)] = f - \bar{e}''(\tau), \tag{6a}$$

$$g[\bar{x}(\tau)] = \begin{cases} \bar{x}(\tau) - 1, & \bar{x}(\tau) < 1, \\ 0, & |\bar{x}(\tau)| \le 1, \\ \bar{x}(\tau) + 1, & \bar{x}(\tau) > 1 \end{cases}, \tag{6b}$$

where $f = F/(k_m b)$, $\bar{k}_a(\tau) = k_a(\tau)/k_m$, and $(\,)'$ denotes differentiation with respect to τ.

One of the main disadvantages of this model is its dependence on the deformable-body model to determine the gear mesh parameters $k(t)$ and $e(t)$. The involute profile modifications are represented in this model by $e(t)$ that corresponds to unloaded *STE*. Hence, a static analysis is performed on the deformable-body model developed for the same gear pair, described in detail in Section 2.1, under unloaded conditions for several discrete positions over a period of one mesh cycle to determine $e(t)$. Similarly, the mesh stiffness function $k(t)$ is obtained from the same static analysis of the deformable-body model, now under operating load conditions. As the gears rotate, the number of teeth in contact changes resulting in time-varying mesh stiffness. This analysis is repeated at the same discrete rotational positions over a mesh cycle to obtain the loaded static transmission error (*LSTE*). This is used to estimate the mesh stiffness at each discrete position *i* as

$$k_i = \frac{T_1}{r_1}\left[\frac{1}{(LSTE - e)_i}\right]. \tag{7}$$

Both $e(t)$ and $k(t)$ are represented in Fourier series form in the model. The nonlinear differential equation of motion (6) is solved numerically by using a fourth order, variable step Runge-Kutta (Dormand-Prince pair) numerical integration routine available in MATLAB.

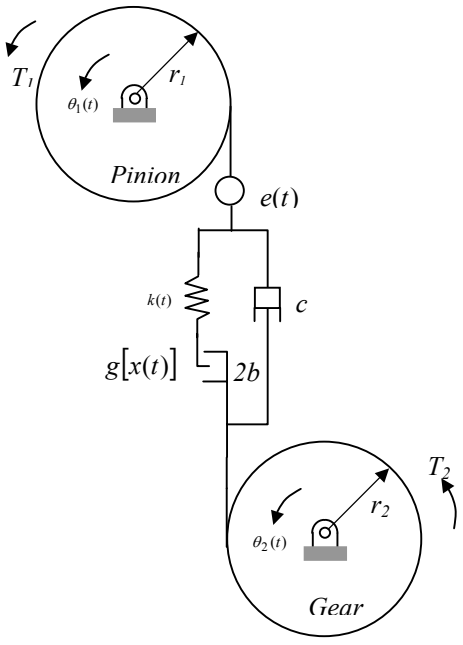

Figure 2: Discrete dynamic model a spur gear pair.

3. Validation of Dynamic Models

3.1. Experimental Study. A power circulation type test machine shown in Figure 3 is employed for the experimental study. The same test machine was used previously to study nonlinear behavior of spur gear pairs including jump discontinuities, parametric resonances and chaotic motions [16-18]. Experimental investigations on the influence of certain design parameters such as tooth profile modifications [19] and contact ratio [20] on the dynamic behavior of spur gear pair were also performed using the same machine.

A detailed description of the test machine can be found in reference [16]. It is of primary interest here to note that the test gear set shown to the left in Fig. 3 are well-isolated from the reaction gear box through massive flywheels, elastomer couplings and flexible shafts, such that influence of the reaction gear pair on the dynamic behavior of the test gear system is negligible. A constant torque is applied to the closed loop thorough a split coupling. Each test gear is assembled on its shaft precisely to avoid any mounting error. A pair of precision spherical roller bearings supports the bearings that are housed in the bearing caps. The bearing caps and the bearings pedestals are such that there are no shaft misalignments. In addition, the bearing pedestals and the bed-plate of the test machine are rigid.

A rotational speed range of 500 to 4000 rpm (415 to 3330 Hz of mesh frequency) is considered for each test. The accelerometer based *DTE* measurement system consists of four diametrically opposed linear accelerometers on each test gear shaft that are mounted near the gear blanks tangentially at a certain radius such that $\ddot{\theta}_1$ and $\ddot{\theta}_2$ can be measured with any gravitational effects cancelled out. These signals are combined using analog circuitry to obtain $d^2(DTE)/dt^2 = r_1\ddot{\theta}_1 + r_2\ddot{\theta}_2$, which is integrated twice to obtain *DTE*. Details of this method and the signal processing can be found in reference [16].

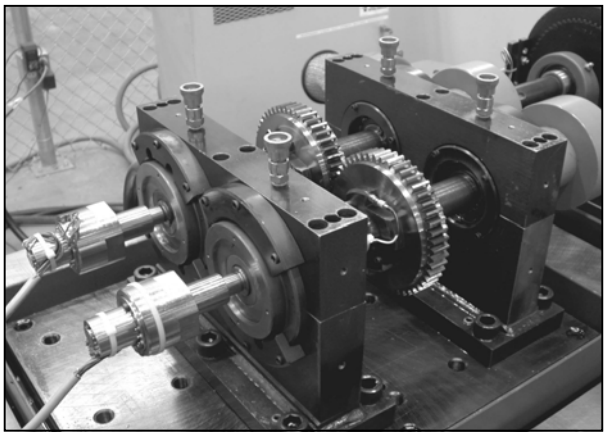

Figure 3: Gear dynamics test machine.

Different sets of spur test gear pairs are considered in the experimental study representing different modification parameters and involute contact ratios (*ICR*). Experimental test matrix covered an *ICR* range between 1.0 and 2.0 as well as different magnitudes of linear profile tip relief ($\delta = 0$, 4 and 10 μm) and different roll angles where the tip relief starts ($\alpha = 20.9^\circ$ representing the pitch point, $\alpha = 22.2^\circ$ near the highest point of single tooth contact, $\alpha = 23.6^\circ$ and $\alpha = 24.8^\circ$). Due to space limitations, this paper will use data from a small subset of this experimental study formed by the three gear pairs shown in Figure 4. Table 1 lists the common gear design parameters of the test gears. Each gear pair is formed by identical gears (unity ratio) and operated at a 150 mm center distance.

Each gear set was tested at several torque levels up to 350 N-m while only the results for 170 Nm and 340 Nm are included in this paper. The rotational speed was varied between 500 and 4000 rpm with an increment of nearly 50 rpm and root-mean-square (rms) value of the measured *DTE* at each speed increment was recorded under steady state conditions. In order to capture jump-up and jump-down type nonlinear phenomena, tests were repeated for both speed-up and speed-down conditions.

Table 1: Common design parameters of the spur gear pairs used for the model validation.

Number of teeth	50
Module, mm	3.0
Pressure angle, deg.	20.0
Pitch diameter, mm	150.0
Base diameter, mm	140.954
Outside diameter, mm	variable
Normal circular tooth thickness, mm	4.64
Helix angle, deg.	0
Tooth profile modifications	variable

Figure 4: The test gear pairs used in this study. (a) $\delta = 0$, $ICR = 1.8$, (b) $\delta = 10\ \mu m$, $\delta = 20.9$ deg, $ICR = 1.8$, and (c) $\delta = 0$, $ICR = 1.4$.

3.2 Comparison of Measured and Predicted *DTE* Values. Dynamic analyses are performed using both models for different sets of gear pairs described in the previous section. The models are validated by comparing the predicted *DTE* values with the measured ones. The deformable-body model for one of the example gear pairs is shown in Figure 1. Lumped inertias were added to the gear inertias to account for the difference in the width between gear teeth and the blank. The Rayleigh damping coefficients were chosen as $\mu = 479$ and $\eta = 1.4(10)^{-7}$ [28] so that the damping ratio is about one percent as determined by the experiments.

In order to capture jump-up and jump-down type nonlinear phenomena as in experiments, simulations were also repeated for both speed-up and speed-down conditions within a range of 500 to 4000 rpm (gear mesh frequency 415 to 3330 Hz) with a increment between 50 to 150 rpm. In order to reach steady state motions, each deformable-body analysis was performed in four different stages. First, the system was ramped up (or down) to the desired speed in a relatively smaller number of very coarse time steps (25 mesh cycles with 8 time-steps per mesh cycle). A second stage of simulation was performed at this constant speed to surpass the transients using a coarse time step (30 to 50 mesh cycles with about 20 time steps per mesh cycle), followed by a more refined third stage (25 mesh cycles with 50 points per mesh cycle) to reach steady state motions. The final stage of simulation used a very small time step (4 mesh cycles with 128 points per mesh cycle) to capture all dynamic motions to the desired resolution. This final section of data was used to extract steady state response. Here, the main reason for performing the last two stages separately was that stress calculations increase the computational time by more than a factor of two. Hence, by enabling stress calculations only in the final stage of analysis, significant amount of computational effort was saved without compromising the required resolution of response. As in the case of an actual speed sweep, the last simulation point of the steady state motion from the previous speed increment was considered as the initial condition for the ramp-up (ramp-down) followed by a refined steady-state simulation.

For the discrete model simulation, gear inertias were calculated using the disk approximation and gear mesh parameters were obtained from the quasi-static analysis of deformable-body model. Speed changes were introduced in sudden step increments. However, since the simulation is extremely fast compared to that of the deformable-body model, a much smaller speed increment was used and the simulation at each speed increment was carried out with a

refined time step (about 125 mesh cycles with 128 points per mesh cycle).

In the deformable-body model, time histories of *DTE* were calculated from the angular displacements of the pinion and gear using eq. (1). Time histories of the dynamic mesh force (*DMF*) were obtained by adding all the individual dynamic tooth forces (*DTF*). Fast Fourier Transform (*FFT*) of the each time history is used to compute the root-mean-square (rms) values of *DTE* and *DMF*. Maximum and minimum principal stresses, σ_{max} and σ_{min}, were computed at several pre-determined root locations ranging from the root center to the start of active profile.

In the case of the discrete model, *DMF* at a given time τ is defined as

$$DMF(\tau) = k_m b \left\{ 2\zeta\, \bar{x}' + [1 + \bar{k}_a(\tau)]\, g[\bar{x}(\tau)] \right\} \qquad (8)$$

Here, it may be noted that the magnitude of the damping force term is very small compared to the stiffness force term and hence may be neglected in the calculation of the total gear mesh force. Individual dynamic tooth forces (*DTF*) were calculated using an approximate formula given by

$$DTF(\tau) = [\frac{STF(\tau)}{SMF}]\, DMF(\tau) \qquad (9)$$

The static tooth force $STF(\tau)$ is obtained from the deformable-body model for one complete mesh cycle under quasi-static conditions.

Data from three gear sets shown in Figure 4 are presented here for validation of the models. In Figure 5 for the first gear pair having no profile modification ($\delta = 0$) and $ICR = 1.8$ at 340 Nm, the rms values of the measured *DTE* are compared to predictions of both models within the entire mesh frequency range of interest. It is observed in Figure 5 that the predictions of the deformable-body model match measured data very well in terms of both overall amplitudes and the shape of the forced response. The measured primary resonance near 3100 Hz as well as the first two super-harmonic resonances near 1550 and 1000 Hz are predicted accurately by the deformable-body model. The amplitudes of the *DTE* are also predicted accurately in both resonance and off-resonance regions. In addition, the measured nonlinear behavior characterized by a frequency range of double stable motions (a lower branch no-contact-loss motion and an upper branch tooth separation motion) bounded by jump-up and jump-down discontinuities also match well with the experimental data. The same conclusions can also be reached for the discrete model with one exception that the *DTE* predictions of this model along the upper branch tooth separation motions are somewhat larger than the experimental data as well as the deformable-body model predictions. This might be because the model shown in Figure 2 is a relatively simple one with many secondary effects neglected including gear blank deflections.

Figures 6 and 7 present the same type of comparison for the other two gear pairs at 340 Nm and 170 Nm respectively. In Figure 6 for a $ICR = 1.8$ gear pair with a linear tip relief of $\delta = 10\ \mu m$ starting at the pitch line ($\alpha = 20.9$ deg roll angle), the nonlinear behavior is significantly less and the forced response is nearly linear. This is attributed to the fact that the applied load of 340 Nm corresponds to the "design load" for the profile modifications made on the gear pair [19]. Because of this, the discrete model compares with experiments as good as the deformable-body model. Meanwhile, the non-linear jump discontinuities due to tooth separations are again evident in Figure 7 for the third gear pair having no profile modifications ($\delta = 0$) but a different involute contact ratio, $ICR = 1.4$ at 170 Nm. Similar to Figure 5, both models compare well with the measured data while the discrete model predicts larger upper branch motions with separations. In addition to the good agreement in terms of the rms values of *DTE*, the harmonic components of predicted *DTE* also compare well with the experiment. Figure 8 illustrates this for the gear pair used in Figure 6 at gear mesh frequencies of 1.5, 2.1 and 2.9 kHz.

Comparisons to experimental data from gear pairs having parameters different from those shown in Figure 4 were also made in this study with the same level of agreement. For instance, gear pairs having different modification amplitudes (say $\delta = 4\ \mu m$) were tested and simulated at torque levels other than the ones considered here to demonstrate that both models are indeed capable of predicting the dynamic response of a gear pair accurately. These additional comparisons can be found in reference [33].

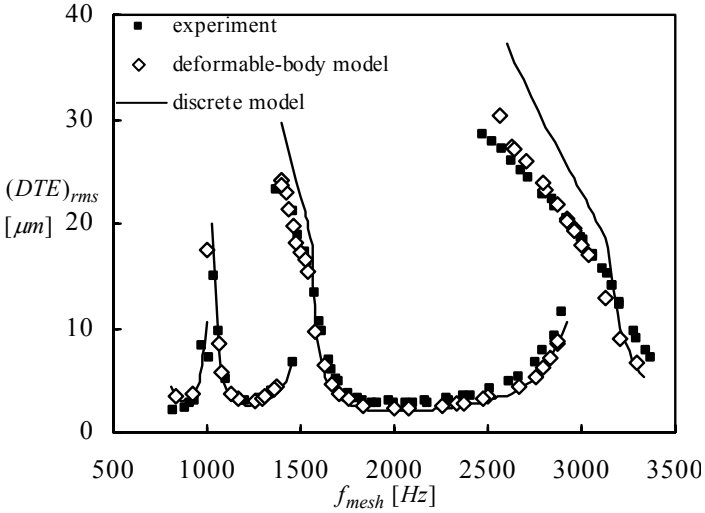

Figure 5: Comparison of measured and predicted rms values of *DTE* for an unmodified gear pair with $\delta = 0$ and $ICR = 1.8$ at 340 Nm.

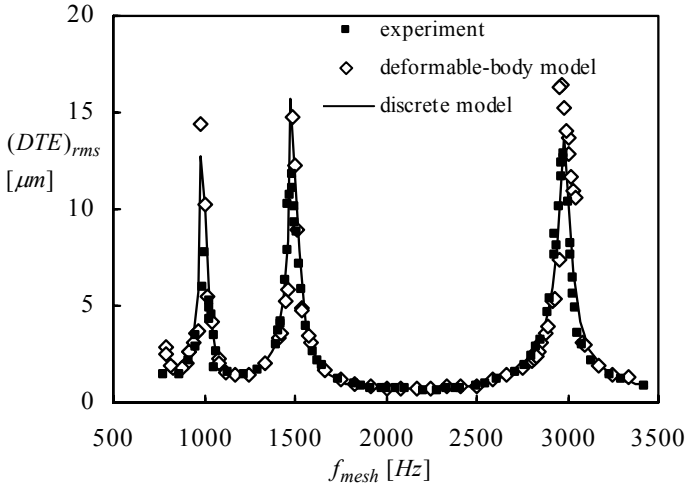

Figure 6: Comparison of measured and predicted rms values of *DTE* for a modified gear pair with $\delta = 10\ \mu m$, $\alpha = 20.9$ deg. and $ICR = 1.8$ at 340 Nm.

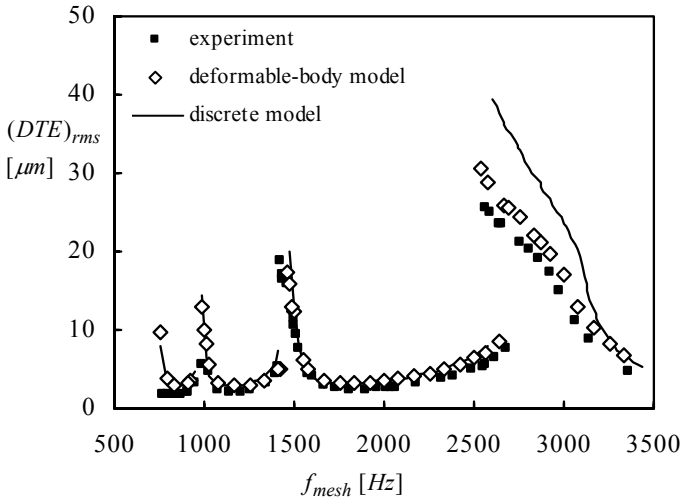

Figure 7: Comparison of measured and predicted rms values of *DTE* for an unmodified gear pair with $\delta = 0$ and $ICR = 1.4$ at 170 Nm.

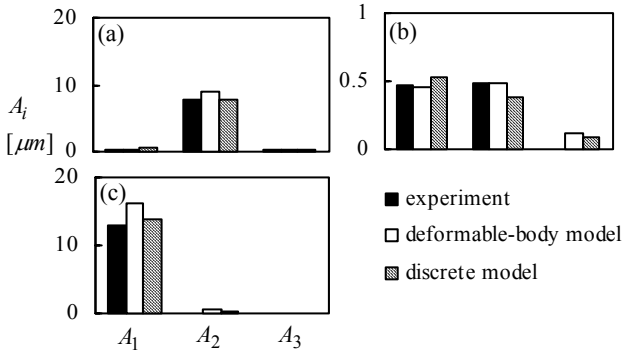

Figure 8: Comparison of the harmonic amplitudes of measured and predicted DTE for $\delta = 10\ \mu m$, $\alpha = 20.9$ deg. and $ICR = 1.8$ at 340 Nm. (a) 1500 Hz, (b) 2100 Hz, and (c) 2900 Hz.

4. Comparison of *DTE* and Different Forms of *DF*

Next, the validated dynamic models introduced earlier will be used to investigate the relationship between the *DTE*, a commonly measured and predicted noise metric, and different forms of dynamic factors that have been used in design to account for the increase in forces and bending stresses due to dynamic effects. Before this can be done, different versions of *DF* will be defined here based on the total gear mesh force, individual tooth forces and the principal bending stresses. The dynamic mesh force factor $(DF)_{mf}$ will be defined as the ratio of the maximum value of the dynamic mesh force in one complete mesh cycle of the steady-state response to the static mesh force:

$$(DF)_{mf} = \frac{(DMF)_{\max}}{SMF} \tag{10a}$$

where $SMF = T_1/r_1 = T_2/r_2 = \text{constant}$. Similarly, the dynamic tooth force factor $(DF)_{tf}$ is the ratio of the maximum value of the dynamic tooth force in one complete mesh cycle of the steady-state response to the maximum value of the static tooth force during the same mesh cycle:

$$(DF)_{tf} = \frac{(DTF)_{\max}}{(STF)_{\max}}. \tag{10b}$$

Finally, the dynamic stress factor $(DF)_{\sigma}$ is defined as the ratio of the maximum value of the dynamic bending stress σ_d on the gear tooth in one complete mesh cycle of the steady-state response to the maximum value of the static bending stress σ_s during one mesh cycle.

$$(DF)_{\sigma} = \frac{(\sigma_d)_{\max}}{(\sigma_s)_{\max}}. \tag{10c}$$

Figures 9, 10 and 11 compare these three types of *DF* predicted by both dynamic models to the predicted *DTE* values for the gear pairs used in Figures 5, 6 and 7, respectively. In these figures, the top figure displays $(DF)_{mf}$, $(DF)_{tf}$ and $(DF)_{\sigma}$ together with *DTE* as predicted by the deformable-body model while the bottom figure shows discrete model predictions of $(DF)_{mf}$, $(DF)_{tf}$ and *DTE*. $(DF)_{\sigma}$ is not included in the bottom figures since the discrete model is not capable of predicting stresses. In Figures 9 to 11, the vertical axis for $(DF)_{mf}$, $(DF)_{tf}$ and $(DF)_{\sigma}$ is shown on the left hand side and the vertical axis for *DTE* is to the right.

Focusing on the deformable-body model predictions first (Figures 9(a), 10(a) and 11(a)), it is seen that (i) values of $(DF)_{tf}$ and $(DF)_{\sigma}$ are very close to each other regardless of the mesh frequency, and (ii) $(DF)_{mf}$ and rms values of *DTE* are proportional to each other. The first observation is somewhat expected since the tooth force and

the resultant bending stress can be considered to be linearly proportional to each other, at least when only the tooth bending effects are considered. It can also be stated that $(DF)_{mf}$ is always significantly larger than both $(DF)_{tf}$ and $(DF)_{\sigma}$. For instance at 2750 Hz in Figure 9, lower branch motion has $(DF)_{tf} \approx (DF)_{\sigma} = 1.1$ and $(DF)_{mf} = 1.4$ while the upper branch motion yields $(DF)_{tf} = 1.8$, $(DF)_{\sigma} = 2.0$ and $(DF)_{mf} = 2.75$. At this frequency, a design based on $(DF)_{mf}$ would be about 30 percent more conservative than that of $(DF)_{tf}$ or $(DF)_{\sigma}$.

A comparison between the predictions of both models in Figures 9 to 11 reveals that the discrete model agrees well with the deformable-body model in predicting *DF*. This has practical consequences since the discrete model is several orders of magnitude faster than the deformable-body model. Also since $(DF)_{tf}$ and $(DF)_{\sigma}$ are rather close to each other, the discrete model can provide a dynamic factor that can be readily used for design purposes.

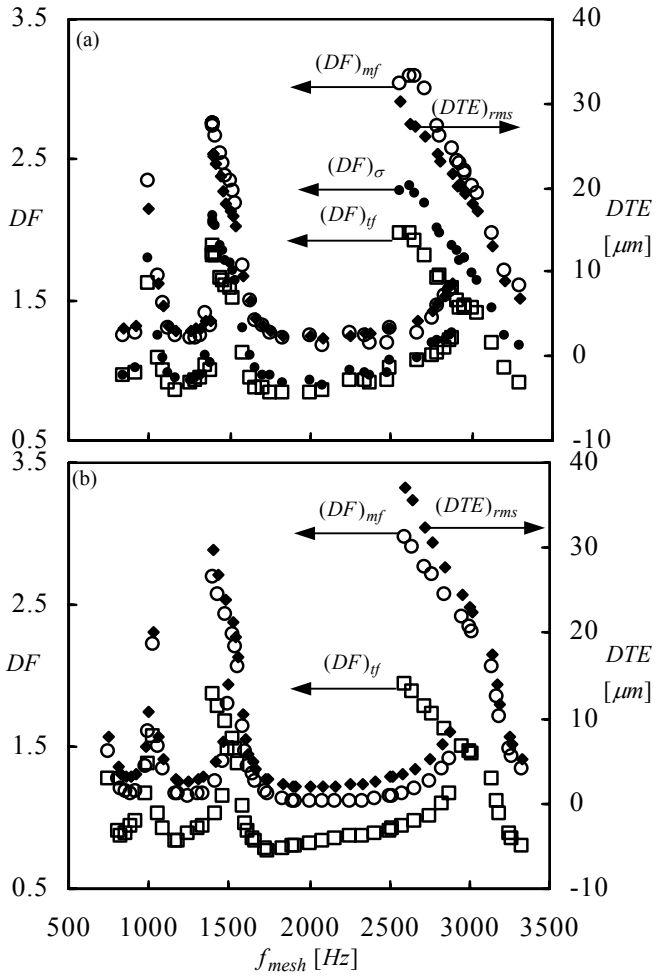

Figure 9: Comparison of $(DF)_{mf}$, $(DF)_{tf}$, $(DF)_{\sigma}$ and $(DTE)_{rms}$ for an unmodified gear pair with $\delta = 0$ and $ICR = 1.8$ at 340 Nm. (a) Deformable-body model and (b) discrete model.

4.1 Relationships Between *DTE* and Different Forms of *DF*. Earlier, *DF* values were shown to follow the same overall trends as *DTE* predictions as the mesh frequency is varied. Here, certain relationships between different forms of *DF* and *DTE* will be sought. If this can be accomplished, measurement of *DTE*, which is in many cases a more feasible task than measurement of DF especially for finer pitch gears, could be used as an indirect measure of DF for design purposes. This would also provide the well-established *DTE* database to be used for durability purposes. Here, an attempt has been made to relate *DTE* to both $(DF)_{mf}$ and $(DF)_{\sigma}$ (and indirectly to $(DF)_{\sigma}$).

For the relationship between *DTE* and $(DF)_{mf}$, half of the peak-to-peak values of *DTE* and *DMF*, denoted by $(DTE)^{o-p}$ and $(DMF)^{o-p}$ were normalized with respect to λ and *SMF*, respectively. Here, λ corresponds to the difference between the average values of *LSTE* and

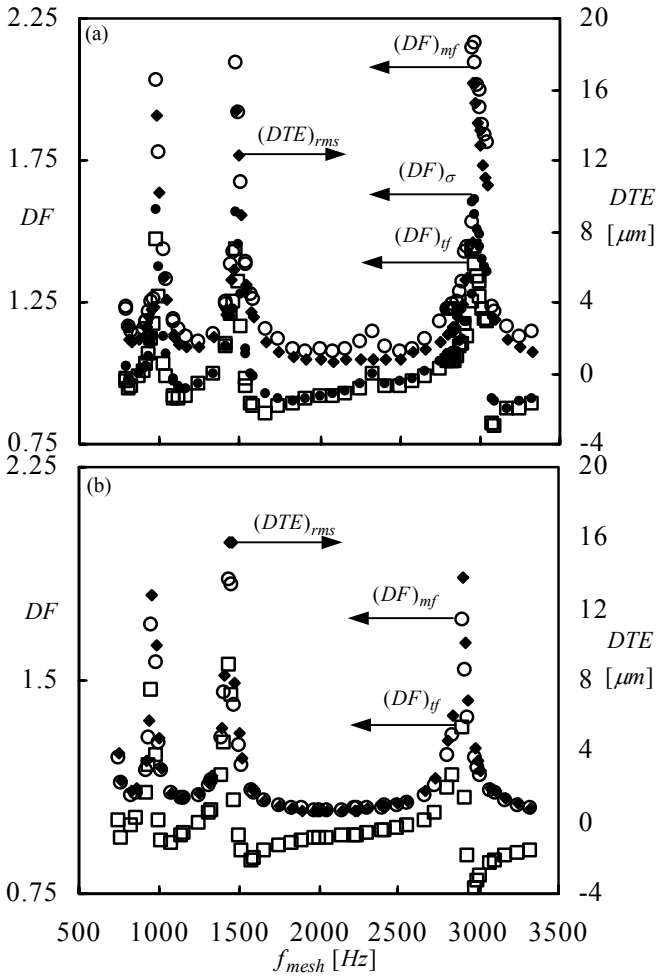

Figure 10: Comparison of $(DF)_{mf}$, $(DF)_{tf}$, $(DF)_{\sigma}$ and $(DTE)_{rms}$ for a modified gear pair with $\delta = 10\ \mu m$, $\alpha = 20.9$ deg. and $ICR = 1.8$ at 340 Nm. (a) Deformable-body model and (b) discrete model.

unloaded *STE* given by $\lambda = (LSTE)_{ave} - e_{ave}$. These two normalized parameters at all mesh frequencies are plotted against each other in Figure 12 for all the three gear pairs considered earlier as predicted by the discrete model. In these figures, the slope for the no contact loss solutions is nearly equal to unity and hence

$$\frac{(DMF)^{o-p}}{SMF} \approx \frac{(DTE)^{o-p}}{\lambda} \tag{11a}$$

Rearranging this equation as

$$\frac{(DMF)^{o-p} + SMF}{SMF} \approx \frac{(DTE)^{o-p}}{\lambda} + 1, \tag{11b}$$

letting $(DMF)^{o-p} + SMF = (DMF)_{\max}$, and using the earlier definition of $(DF)_{mf}$ given by eq. (10a), one writes the first relationship of interest as

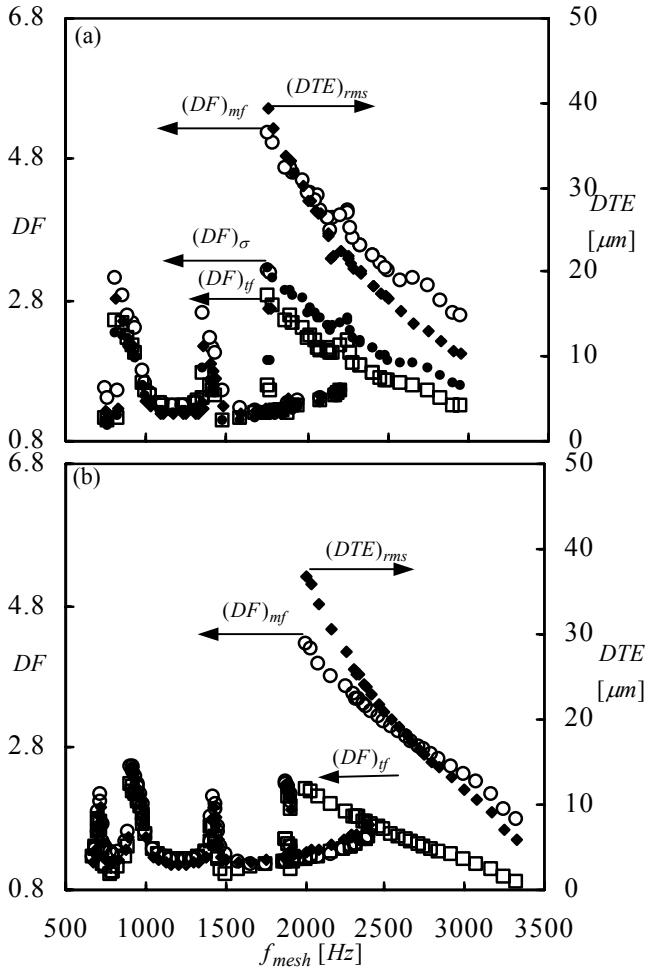

Figure 11: Comparison of $(DF)_{mf}$, $(DF)_{tf}$, $(DF)_{\sigma}$ and $(DTE)_{rms}$ for an unmodified gear pair with $\delta = 0$ and $ICR = 1.4$ at 170 Nm. (a) Deformable-body model and (b) discrete model.

$$(DF)_{mf} \approx \frac{(DTE)^{o-p}}{\lambda} + 1. \tag{12}$$

This relationship between $(DF)_{mf}$ and *DTE* is quite accurate in the linear frequency regime when no contact loss occurs, but would give a conservative estimate $(DF)_{mf}$ in the non-linear regime. This is evident in Figures 12(a) and 12(c) for the regions of tooth separation where the slope is nearly one-half. As a matter of fact, eq. (11a) can be rewritten as

$$(DMF)^{o-p} \approx [\frac{SMF}{\lambda}](DTE)^{o-p} \tag{13}$$

where the slope can be physically interpreted as the average value of stiffness. In the non-linear region, because the teeth separate during a portion of the mesh cycle, the average value of stiffness is reduced. Hence the decrease in slope observed in Figures 12(a) and 12(c) should be expected.

The second relationship between $(DF)_{\sigma}$ and *DTE* is illustrated with the help of Figures 13(a-c) obtained by using the predictions of the deformable body model for the same three gear pairs. These figures plot $(DF)_{\sigma}$ against $(DTE)_{\max}$ that is normalized with respect to $(LSTE)_{\max}$. Figures 13 demonstrate a direct linear relationship between these two parameters such that

$$(DF)_{\sigma} \approx \frac{(DTE)_{\max}}{(LSTE)_{\max}} \tag{14}$$

This relationship provides a very good approximation for $(DF)_{\sigma}$ in both linear and nonlinear regimes and can be used for design purposes in estimating $(DF)_{\sigma}$ from *DTE*.

5. Conclusion

In this study, two different dynamic models of varying complexity were developed and validated by comparing the predicted *DTE* values to the available experimental data. The deformable-body model is capable of predicting *DTE*, tooth forces as well as the tooth bending stresses. The discrete model uses the results from the quasi-static analysis of the deformable-body model to predict the *DTE*, and gear mesh and tooth forces. Three different dynamic factors were defined and their values were compared with that of *DTE* in both linear and nonlinear motion regimes. Dynamic factors based on tooth forces and bending stresses were shown to be approximately equal while dynamic factors based on total gear mesh forces are consistently higher that the other two types of dynamic factors. At the end, simple design formulas were proposed to relate *DTE* to dynamic factors based on gear mesh forces and stresses.

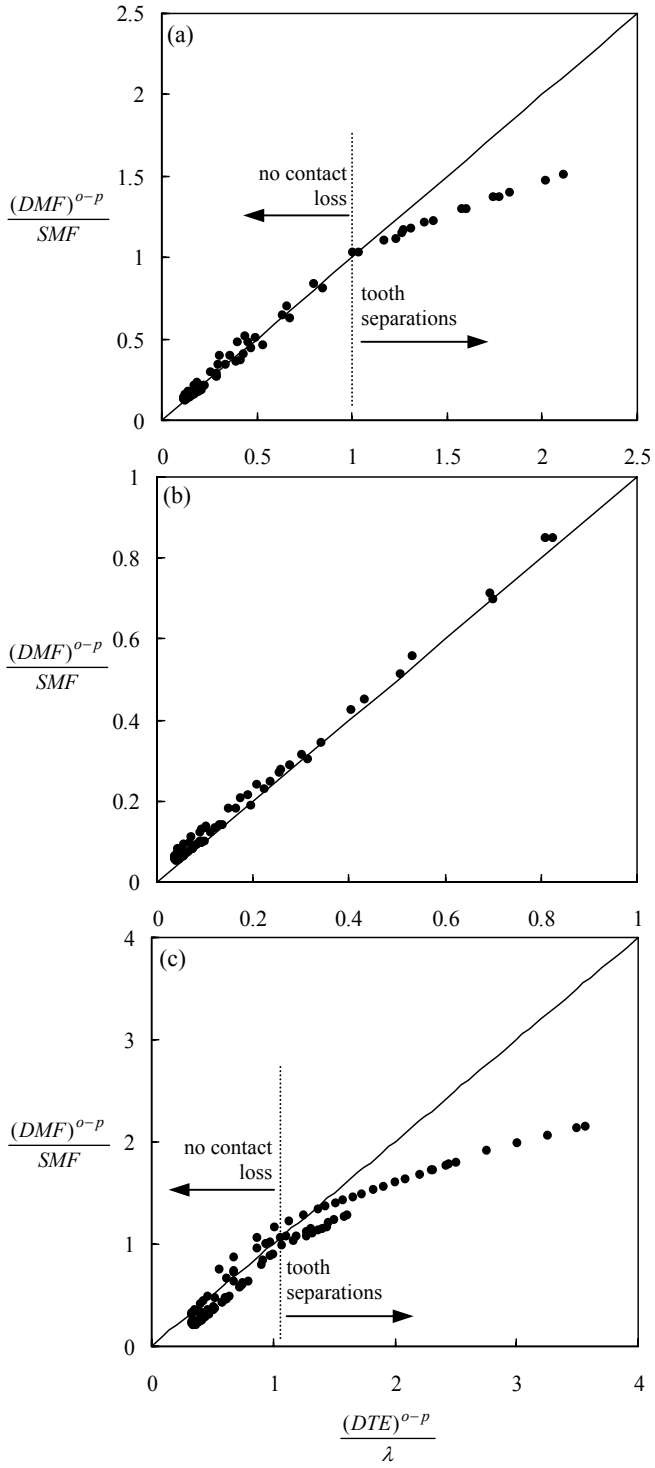

Figure 12. Normalized values of $(DMF)^{o-p}$ versus $(DTE)^{o-p}$ for (a) $\delta = 0$, $ICR = 1.8$, (b) $\delta = 10\ \mu m$, $\alpha = 20.9$ deg, $ICR = 1.8$, and (c) $\delta = 0$, $ICR = 1.4$.

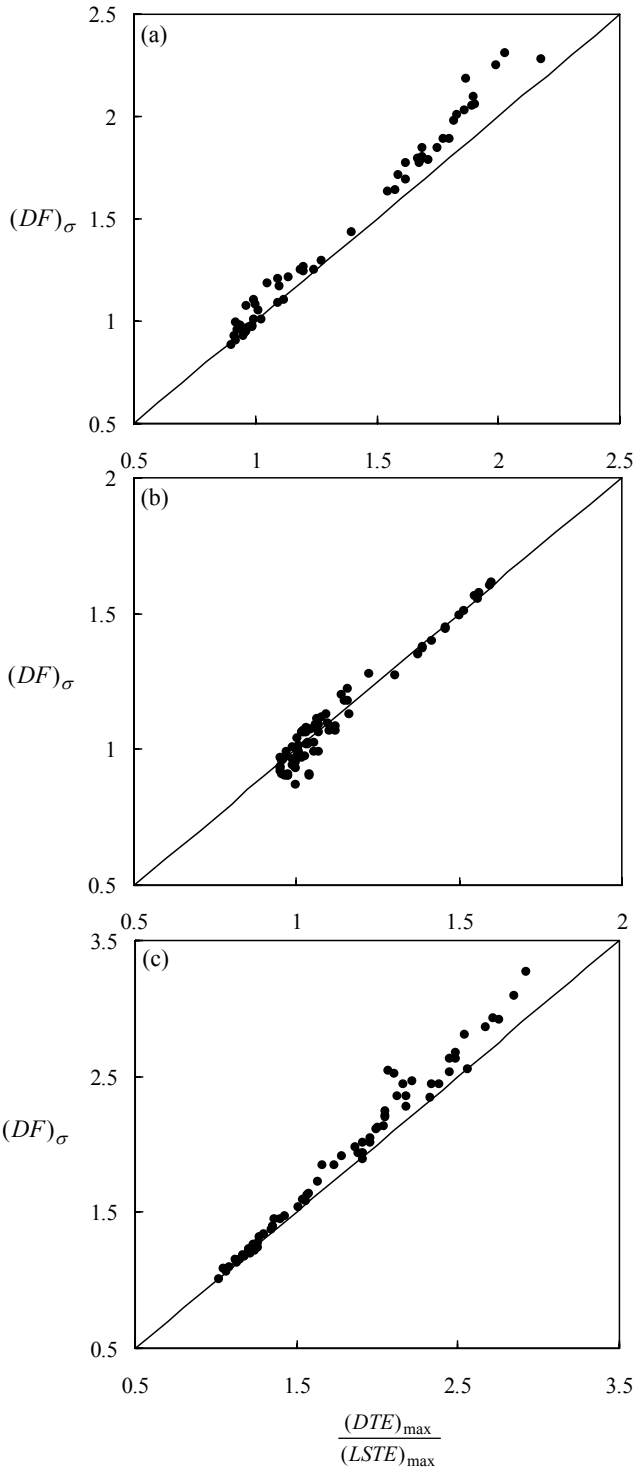

Figure 13: $(DF)_\sigma$ versus $(DTE)_{\max}$ for (a) $\delta = 0$, $ICR = 1.8$, (b) $\delta = 10\ \mu m$, $\alpha = 20.9$ deg, $ICR = 1.8$, and (c) $\delta = 0$, $ICR = 1.4$.

References

[1] American National Standard, "Fundamental Rating Factors and Calculation Methods for Involute Spur and Helical Gear Teeth," *AGMA Standard, ANSI/AGMA 2001-C95*.

[2] Ozguven, H. N. and Houser, D. R., 1988, "Mathematical Models Used in Gear Dynamics - A Review," *Journal of Sound and Vibration*, **121**, 383-411.

[3] Blankenship, G. W. and Singh, R., 1992, "A Comparative Study of Selected Gear Mesh Interface Dynamic Models" ASME International Power Transmission and Gearing Conference, DE 43-1.

[4] Wang, J., Li, R. and Peng, X., 2003, "Survey of Nonlinear Vibration of Gear Transmission Systems," Appl Mech Rev, **56 (3)**, 309-329.

[5] Kahraman, A., Ozguven, H. N., Houser, D. R., and Zakrajsek, J. J., 1992, "Dynamic Analyses of Geared Rotors by Finite Elements," *ASME Journal of Mechanical Design*, **114**, p507-514.

[6] Ozguven, H.N. and Houser, D.R., 1988, "Dynamic Analysis of High Speed Gears by Using Loaded Static Transmission Error," *Journal of Sound and Vibration*, **125**, 71-83.

[7] Ozguven, H. N., 1991, "A Non-linear Mathematical Model for Dynamic Analysis of Spur Gears Including Shaft and Bearing Dynamics," *Journal of Sound and Vibration*, **145**, 239-260.

[8] Kahraman, A. and Singh, R. 1990, "Non-linear Dynamics of a Spur Gear Pair," *Journal of Sound and Vibration*, **142**, 49-75.

[9] Amabili, M. and Rivola, A., 1997, "Dynamic Analysis of Spur Gear Pairs: Steady-State Response and Stability of the SDOF Model with Time-varying Mesh Damping," *Mechanical Systems and Signal Processing*, **11**, 375-390.

[10] Huang, K. J. and Liu, T. S., 2000, "Dynamic Analysis of a Spur Gear by the Dynamic Stiffness Method," *Journal of Sound and Vibration*, **234**, 311-329.

[11] Theodossiades, S. and Natsiavas, S., 2000, "Non-linear Dynamics of Gear-pair Systems with Periodic Stiffness and Backlash," *Journal of Sound and Vibration*, **229**, 287-310.

[12] Maliha, R., Dogruer, U. and Ozguven, H. N., 2004, "Nonlinear Dynamic Modeling of Gear-Shaft-Disk-Bearing Systems using Finite Elements and Describing Functions," *ASME Journal of Mechanical Design*, **126**, 534-541.

[13] Blankenship G. W. and Singh, R., 1995, "A New Gear Mesh Interface Dynamic Model to Predict Multi-Dimensional Force Coupling and Excitation," *Mechanism and Machine Theory*, **30**, 43-57.

[14] Munro, R. G., 1962, *Dynamic Behaviour of Spur Gears*, Ph.D. Dissertation, Cambridge University.

[15] Umezawa, K., Sata, T. and Ishikawa, J., 1984, "Simulation of Rotational Vibration of Spur Gears," *Bulletin of JSME*, **38**, 102-109.

[16] Blankenship, G. W. and Kahraman, A., 1995, "Steady State Forced Response of a Mechanical Oscillator with Combined Parametric Excitation and Clearance Type Nonlinearity," *Journal of Sound and Vibration*, **185**, 743-765.

[17] Kahraman, A. and Blankenship G. W., 1996, "Interactions between Commensurate Parametric and Forcing Excitations in a System with Clearance," *Journal of Sound and Vibration*, **194**, pp. 317-336.

[18] Kahraman, A. and Blankenship, G. W., 1997, "Experiments on Nonlinear Dynamic Behavior of an Oscillator with Clearance and Time-varying Parameters," *ASME Journal of Applied Mechanics*, **64**, 217-226.

[19] Kahraman, A. and Blankenship, G. W., 1999, "Effect of Involute Tip Relief on Dynamic Response of Spur Gear Pairs," *ASME Journal of Mechanical Design,* **121**, 313-315.

[20] Kahraman, A. and Blankenship, G. W., 1999, "Effect of Involute Contact Ratio on Spur Gear Dynamics," *ASME Journal of Mechanical Design*, **121**, 112-118.

[21] Kasuba, R. and Evans, J. W., 1981, " An Extended Model for Determining Dynamic Loads in Spur Gearing," *ASME Journal of Mechanical Design*, **100**, 69-76.

[22] Wang, C. C., 1985, "On Analytical Evaluation of Gear Dynamic Factors Based on Rigid Body Dynamics," *Journal of Mechanisms, Transmissions and Automation in Design*, **107**, 301-311.

[23] Lin, H. H., Oswald, F. B. and Townsend, D. P., 1994, " Dynamic loading of Spur Gears with Linear or Parabolic Tooth Profile Modifications," *Mechanism and Machine Theory*, **29 (8)**, 1115-1129.

[24] Liou, C. H., Lin, H. H., Oswald, F. B. and Townsend, D. P., 1996, " Effect of Contact Ratio on Spur Gear Dynamic Load With No Tooth Profile Modifications," *Journal of Mechanical Design*, **118**, 439-443.

[25] Yoon, K. Y. and Rao, S. S., 1996, " Dynamic Load Analysis of Spur Gears Using a New Tooth Profile," *ASME Journal of Mechanical Design*, **118**, 1-6.

[26] Vedmar, L. and Henriksson, B., 1998, " A General Approach for Determining Dynamic Forces in Spur Gears," *ASME Journal of Mechanical Design*, **120**, 593-598.

[27] Vedmar, L. and Andersson, A., 2003, " A Method to Determine Dynamic Loads on Spur Gear Teeth and on Bearings," *Journal of Sound and Vibration*, **267**, 1065-1084.

[28] Parker, R. G., Vijayakar, S. M, and Imajo, T., 2000, "Non-linear Dynamic Response of a Spur Gear Pair: Modeling and Experimental Comparison," *Journal of Sound and Vibration*, **237**, 435-455.

[29] Kubo, A., Yamada, K., Aida, T., and Sato, S., 1972, "Research on Ultra High Speed Gear Devices," *Transaction of JSME*, **38**, 2692-2715.

[30] EXTPAIR-2D User's Manual, Advanced Numerical Solutions, Inc, 2004.

[31] Vijayakar, S., Busby, H. R., and Houser, D. R., 1987, "Finite Element Analysis of Quasi-prismatic Bodies Using Chebyshev Polynomials," *International Journal of Numerical Methods in Engineering*, **24**, 1461-1477.

[32] Yuksel, C. and Kahraman, A., 2004, " Dynamic Tooth Loads of Planetary Gear Sets Having Tooth Profile Wear," *Mechanism and Machine Theory*, **39**, 695-715.

[33] Tamminana, V. K. "A Study on the Relationship Between the Dynamic Transmission Error and Dynamic Factors of a Spur Gear Pair," M.S. Thesis, The Ohio State University, Columbus, Ohio, 2005.